

Conversion of highly coherent XeCl-laser radiation through the SRS in gaseous hydrogen

N.G. Ivanov, V.F. Losev, and V.E. Prokop'ev

*Institute of High-Current Electronics,
Siberian Branch of the Russian Academy of Sciences, Tomsk*

Received September 2, 1999

In this paper we present some results of the experimental study on the conversion of highly coherent XeCl-laser radiation by use of the SRS process in compressed gaseous hydrogen. About 70 rotational-vibrational components were obtained with the use of a circularly polarized pump beam. It is shown in the paper that the axial vibrational components possess high spatial and temporal coherence under conditions of phase locking in four-wave mixing processes. In the case of only Raman conversion the quantum efficiency into the first vibrational Stokes component was 95%.

1. Introduction

Extending the spectral region of existence of coherent radiation has always been an urgent problem. In recent years this problem has often been solved by nonlinear conversion of single-frequency or two-frequency radiation in hydrogen.¹⁻⁵ This nonlinear medium has an advantage over other such media that the spectrum of radiation converted through the SRS on the rotational-vibrational transitions of hydrogen can have a rich spectrum. The coherence of converted radiation must be very high in this case. On the one hand, hydrogen as a gas is optically homogeneous medium, and therefore at strictly directed pump radiation we can expect high spatial coherence of the converted radiation as well. At the same time, at not very high pressure of hydrogen (2 to 5 atm) high temporal coherence can be obtained due to collisional narrowing of lines of spontaneous Raman scattering (Dicke effect).

The conversion of radiation through the SRS is always accompanied by competition among different nonlinear effects. The most significant phenomenon for hydrogen is four-wave mixing (FWM). As shown in Refs. 1 and 6, the role of FWM increases as the normalized frequency detuning $\gamma = \Delta k / gI_p$ decreases (I_p is the pump intensity, g is the SRS gain factor, Δk is the difference between wave vectors due to the effect of linear dispersion). Nevertheless, according to calculations made in Ref. 7, 100% quantum efficiency of conversion into that or another vibrational component of the SRS spectrum is possible with a plane pump wave under conditions of cascade amplification of the Stokes "seed." To eliminate the influence of mixing processes, which redistribute the energy among the interacting waves, the authors recommend to use the pump intensity not higher than 50 MW/cm² and the hydrogen pressure no less than 10 atm. In practice⁸⁻¹² focused beams are often used for pumping. Besides, their divergence far exceeds the diffraction limit. In this case it is impossible to exclude the influence of mixing processes regardless of the hydrogen pressure. Because of inhomogeneous wave front the spatial distribution of the radiation

intensity in the focal caustic is also inhomogeneous. As a result, conditions for linear and nonlinear phase matching are fulfilled in the spatial region of nonlinear interaction.¹ This is caused by the fact that the parameter γ is close to zero for many microregions. Consequently, the influence of the mixing processes can be decreased only due to a decrease in the divergence of the pump beam at a simultaneous increase in the caustic length.

As was shown in Ref. 1, for Raman conversion in the case of two-frequency pumping the spectral region $\Delta\omega$ including shifted frequencies may be compared with the frequency of the pump radiation ($\Delta\omega \sim \omega_0$). Besides, Losev and Lutsenko¹ have analytically and experimentally shown that the number of spectral components increases with the increasing intensity of the "seed" Stokes signal. However, in practice the ratio of its intensity to the intensity of pump radiation remains to be low (1/50 – 1/30). Hopefully, the conditions close to two-frequency excitation can be realized in one cell when using a long conversion length and sufficiently high intensity of single-frequency pump radiation.

In this paper we consider some possibilities of extending the spectrum of converted radiation. To do this, we propose to use highly coherent single-frequency UV radiation for pumping of hydrogen, while simultaneously choosing proper geometry of the pump radiation focusing and the state of its polarization.

2. Experimental setup

As a source of UV radiation, we used two XeCl* laser systems. The first of them, which is described in a more detail in Ref. 13, was a set of two electric-discharge lasers: master oscillator (MO) and controlled laser operating in the injection seeded mode. In this case the output radiation had the following parameters: energy $e \leq 110$ mJ, pulse length at halfmaximum $\tau = 120$ ns, line width $\Delta\nu = 0.01$ cm⁻¹ (regime II). Without the MO the line width broadened to 100 cm⁻¹, all other parameters being the same. The second system also included the same master oscillator and the second laser capable of operating either in the injection seeded mode (regime I) or as a three-pass amplifier

(regime III). The output laser beam of this system in both cases was characterized by the pulse duration of 20 ns and energy of 55 mJ. The spectrum width varied from 0.01 to 0.1 cm^{-1} depending on whether a Fabry-Perot etalon was installed or not in the cavity of the master oscillator. The output radiation in the regimes I and II was depolarized, and in the regime III it had linear or circular polarization. The angular distributions of radiation in different regimes of operation of the laser systems are shown in Fig. 1. The angle $\Theta_d = 2.44 \lambda / D$ (λ is the radiation wavelength; D is the laser beam diameter) corresponds to the angular size of the first minimum in the directional pattern of the radiation having homogeneous intensity distribution in the near zone. The radiation was focused inside the cell by one or two lenses with the focal lengths $f = 55$ and -20 cm. The cell was made from a stainless steel tube 3 m long; it was possible to change the hydrogen pressure in the cell from 0 to 50 atm. The recording equipment included an IMO-2N power meter, a 6LOR-4 oscilloscope, FEK-22SPU photodiodes, an IT-28-30 Fabry-Perot interferometer, a STE-1 spectrograph, and an IFO-451 microphotometer. The measurement accuracy was 1 ns for temporal characteristics, 1 cm^{-1} for spectral line positions, and 0.01 cm^{-1} for line width.

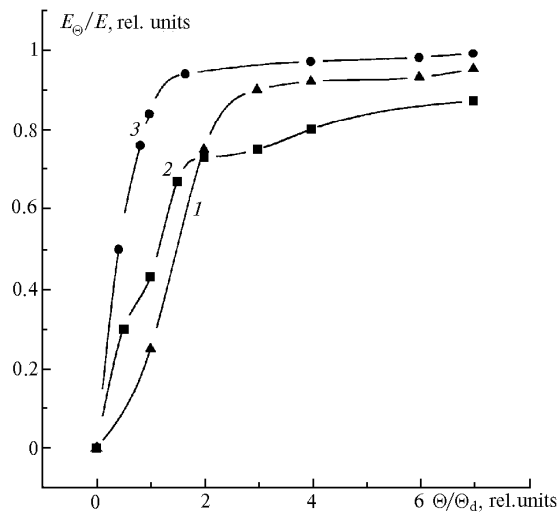


Fig. 1. Angular distribution of the pump radiation in different regimes of operation of the laser systems: injection seeded regime I with: $E_p = 35 \text{ mJ}$, $\tau = 20 \text{ ns}$, $\Delta\nu = 0.1 \text{ cm}^{-1}$, beam size $A = 1.5 \times 3.2 \text{ cm}$ (curve 1); injection seeded regime II with: $E_p = 30 \text{ mJ}$, $\tau = 120 \text{ ns}$, $\Delta\nu = 0.01, 0.1, 100 \text{ cm}^{-1}$, $A = D = 1.2 \text{ cm}$ (curve 2); regime III of three-pass amplification with: $E_p = 25 \text{ mJ}$, $\tau = 20 \text{ ns}$, $\Delta\nu = 0.01$ and 0.1 cm^{-1} , $A = 1.0 \times 0.8 \text{ cm}$ (curve 3).

3. Experimental results

3.1. Conversion efficiency

The dependence of the conversion efficiency on the hydrogen pressure and focusing geometry was studied in a more detail for SRS on the vibrational transitions in the pumping regime I. Figure 2a shows the quantum efficiency of conversion into different Stokes components at the focusing length $f = 7 \text{ m}$. The separate dots show

the efficiency obtained in the pumping regime II. The conversion efficiency was determined from the ratio of the energy of a converted spectrum component to the pump energy after passage of the complete optical path without a cell with hydrogen. Every point in the plots was taken as a statistically mean value over 10 measurements.

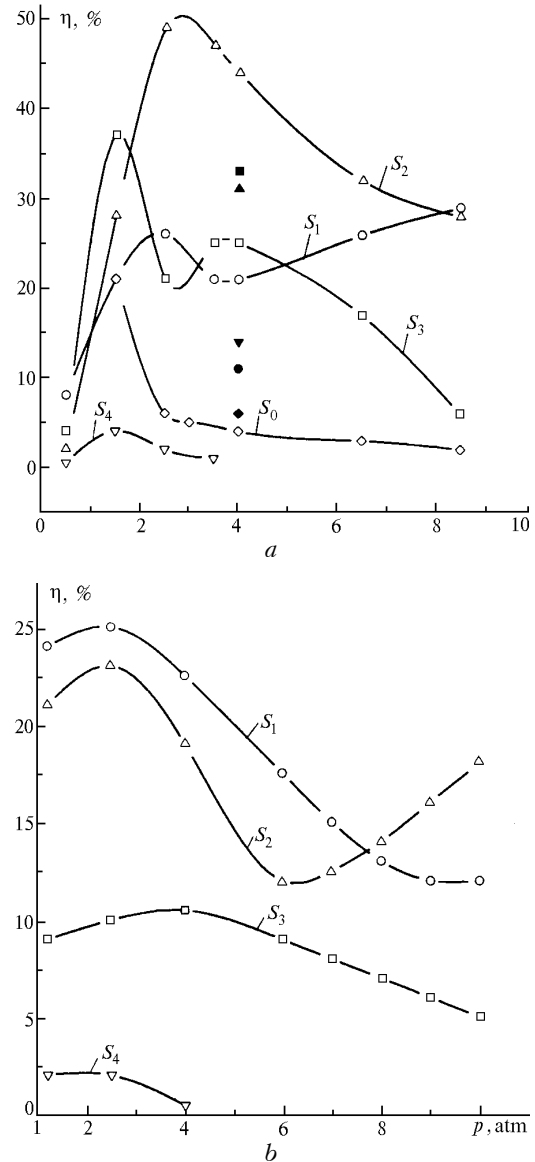


Fig. 2. Quantum efficiency of the conversion into vibrational components vs. hydrogen pressure at focused (a) and collimated (b) pump beams; $S_0, S_1, S_2, S_3,$ and S_4 are, respectively, the fractions of passed through pump radiation and the first, second, third, and fourth Stokes components.

According to theoretical findings from Ref. 7, to eliminate the influence of mixing processes at the cascade SRS, the wave front of the pump radiation should be close to plane. The results of our attempt to obtain this in practice are shown in Fig. 2b. The mean intensity of the collimated pump beam I_p in this case was $\cong 60 \text{ MW/cm}^2$.

As follows from the dependences shown, the efficiency of conversion into the higher Stokes components decreases with the increasing pressure starting from 3 to 4 atm. The fraction of the pump energy that passes through the cell decreases simultaneously. One of the probable channels of the energy loss can be stimulated Rayleigh scattering¹⁴ that propagates at large angles. As seen from Fig. 2a, the efficiency of conversion into the high Stokes components increases as the divergence of the pump beam decreases. Comparing the dependences shown in Figs. 2a and b, we can see that the efficiency of conversion into each Stokes component is lower at pumping by a collimated beam. The total quantum efficiency in this case decreases roughly from 93 down to 60%.

3.2. Spectral characteristics

The spectrum of converted radiation under our conditions depended mostly on the intensity of pump radiation and the state of its polarization. In the experiments the pump intensity varied due to varying focusing length (from 3 to 30 m) and the pump pulse duration.

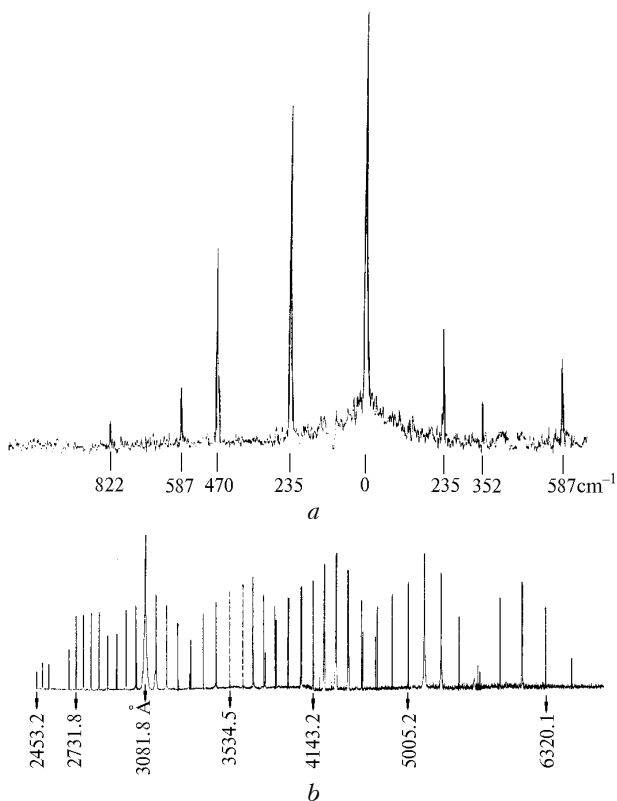


Fig. 3. Densitograms of the spectrum of the converted radiation at linear (a) and circular (b) polarization of the pump radiation: the portion of spectrum nearby 414 nm, the central frequency S_2 ($J = 1 \rightarrow J = 1$) (a); the spectrum recorded in the pumping regime III and $f = 6$ m (b).

At linear polarization and maximum intensity of the pump radiation, the converted spectrum included four Stokes and two anti-Stokes components of the SRS on the vibrational transitions in hydrogen (VSRS). Near each

Stokes component we observed intense satellites on the short-wave side (or on the long-wave side for the anti-Stokes components) at the distance $\Delta\Omega = 234.9 \text{ cm}^{-1}$ (Fig. 3). These satellites occurred due to scattering of the previous component or pumping of the hydrogen molecule in its first excited vibrational state. Under these conditions, in spite of linear polarization of the pump radiation, stimulated scattering on VSRS lines and their more intense satellites occurred at the rotational transition $J = 1 \rightarrow J = 3$ ($\Delta\Omega = 587 \text{ cm}^{-1}$). Besides the above-listed lines, lines caused by sum-frequency conversion were also present in the spectrum.

As the focusing length increased, the intensity of the anti-Stokes vibrational components decreased, as well as the intensity of the corresponding satellites. Thus, only VSRS lines were observed at $f = 4.5$ m in the pump regime II and at $f = 6$ m in the regime III. Their width followed the width of the pump line no matter whether it was wide or as narrow as possible. Such a behavior is not always typical of other nonlinear media.¹³ As an illustration, Fig. 4 shows the fragment of the interferogram of radiation at $\lambda = 500$ and 632 nm at $\Delta\nu_p = 0.01 \text{ cm}^{-1}$. As the background level increased, the converted radiation had a wide-band component at narrow-band pumping due to its amplification in the field of the narrow-band and strictly directed part of the pump radiation. Pump frequency tuning from 0–1 to the 0–2 laser transition resulted in the corresponding tuning of line frequencies in the converted spectrum. As f exceeded some optimal value, the higher Stokes components started to decrease.

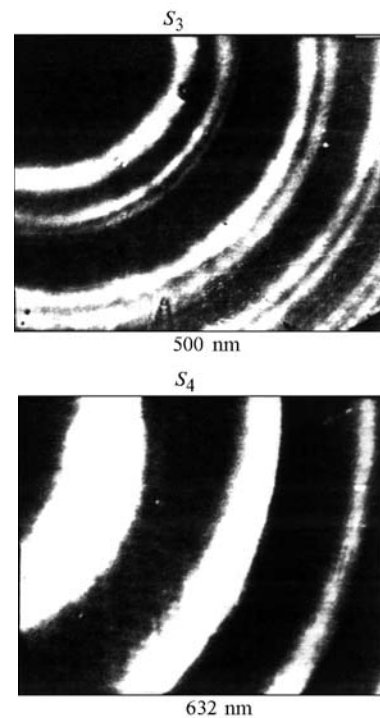


Fig. 4. Fragments of the interferograms of the converted radiation. Free spectral range of the interferometer was 2.14 GHz. The pump radiation at $\lambda = 500$ nm included two narrow-band components.

The spectral composition of this pattern did not change, if the pump radiation was depolarized or had linear polarization. At circular polarization of the pump radiation (possibly, the polarization was slightly elliptical) the spectrum changed significantly. Thus, satellites of the VSRS lines disappeared at a short focusing length, except for lines caused by scattering on the rotational transitions (RSRS). Figure 5 shows the spectrogram with simultaneously recorded spectra at a linear and a circular polarization of the pump radiation, all other conditions being the same.

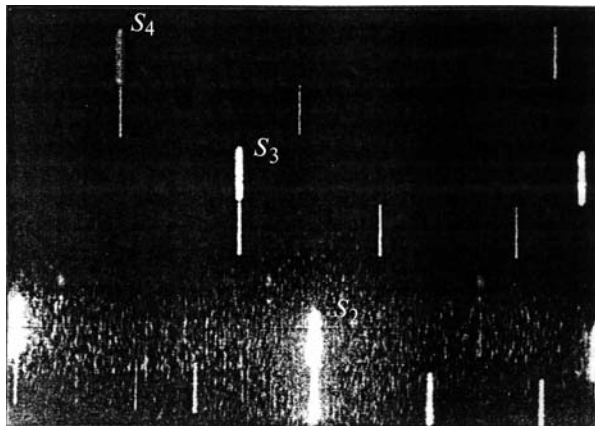


Fig. 5. The spectrogram of the converted radiation at a linearly and a circularly polarized pump radiation.

The maximum number of RSRS lines was observed under the conditions optimal for appearance of the higher vibrational Stokes components. The scattering spectrum in this case occupied the region from UV to the IR, which is almost completely filled with rotational-vibrational components (Fig. 3b). Unfortunately, the RF-3 photographic film we used in the experiments has low sensitivity in the red region and correspondingly underestimated the intensity of radiation at $\lambda > 600$ nm. The lines due to the transition $J = 0 \rightarrow J = 2$ ($\Delta\Omega = 354.4 \text{ cm}^{-1}$) were observed near the strongest Stokes lines of the transition $J = 1 \rightarrow J = 3$ (the region nearby 414 nm).

3.3. Spatial and temporal characteristics

As was already mentioned, the relation between the SRS and FWM processes is determined by the parameter γ , the value of which may be different depending on the geometry of pump radiation focusing, its divergence, and the pressure of hydrogen. The spatial distribution of converted radiation depended, in our experiments, on the process that prevailed in each particular case.

Photographs of the spectrally separated spots of radiation of the vibrational components were taken at the focusing length $f = 4.5$ m, $\tau = 120$ ns, and pressure $p = 4$ atm (Fig. 6). The presence of pronounced core spots and rings of different diameter is characteristic of the higher Stokes components. As follows from Fig. 7a, the divergence of the part of radiation forming the core spot is close to the diffraction limit for all the three

higher Stokes components S_2 , S_3 , and S_4 . As the hydrogen pressure or the pump intensity increased, at the same focusing length, the spot became less pronounced and inhomogeneous and its divergence increased significantly (Fig. 7b).

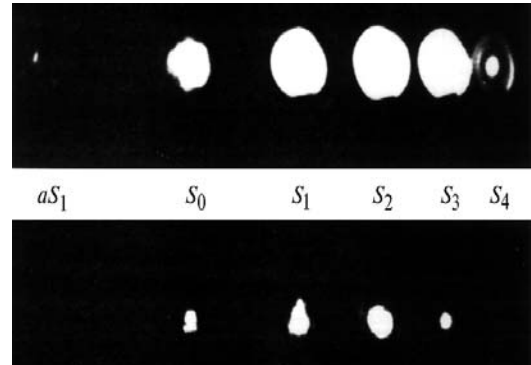


Fig. 6. Photographs of the spectrally separated spots of radiation at the output from the cell filled with hydrogen at different attenuation.

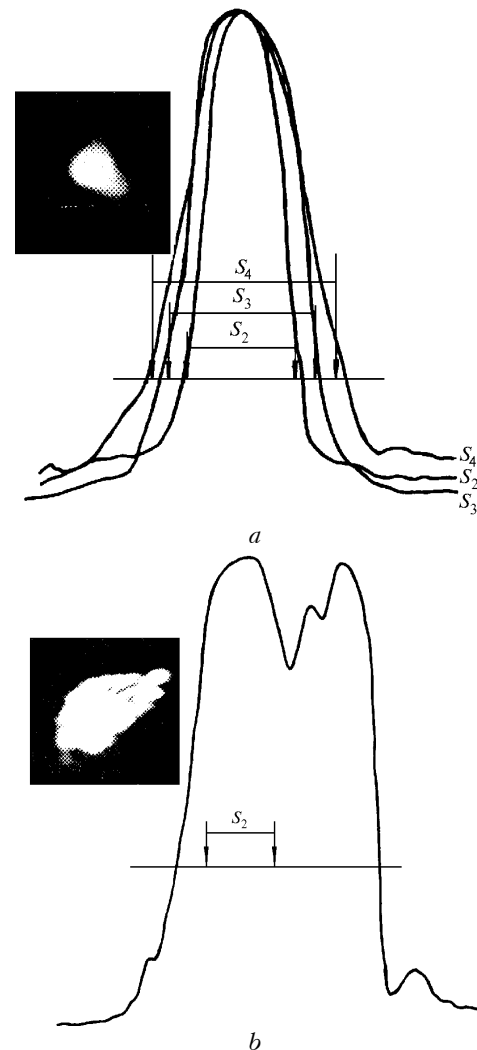


Fig. 7. Densitograms of the focal light spots of S_2 , S_3 , and S_4 components at the hydrogen pressure of 4 (a) and 8 atm (b). The lower straight line shows the level of the second maximum in the Airy pattern; the arrows show the size of the first minimum.

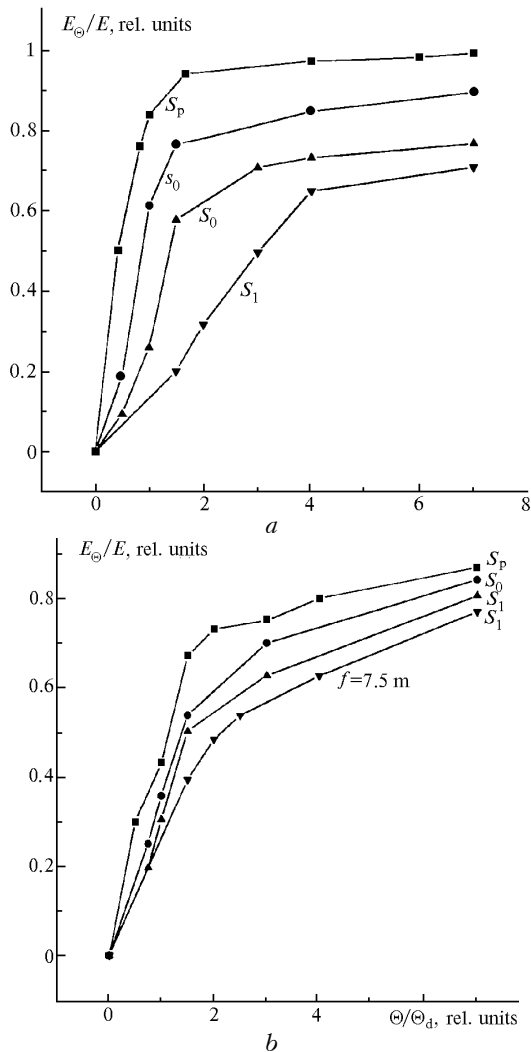


Fig. 8. Angular distribution of the incident pump radiation (S_p), pump radiation after passing the cell (S_0, s_0), first vibrational Stokes component (S_1) at a short (*a*) and long (*b*) pump pulse. The hydrogen pressure $p = 8$ atm; s_0 is for pumping below the SRS threshold.

The growth of γ led to a decreased influence of the mixing processes. Toward this end, the radiation was focused inside the cell filled with hydrogen with a two-component optical system having small numerical aperture. In this case the pump beam was close to a collimated one: the beam diameter was 2 mm at the entrance and exit of the cell and 1 mm at the center of the cell. In this geometry for the regimes II and III and hydrogen pressure of 8 atm, only the pump radiation and the first Stokes component were observed at the output of the cell, and their energies were as follows: 9 and 8 mJ at $\tau = 120$ ns, and 2.5 and 12.5 mJ at $\tau = 20$ ns (minimum divergence of the pump radiation). In spite of a significant energy transfer from the pump radiation to S_1 , in both of the cases we did not observe further cascade conversion. Note that the threshold for appearance of S_1 at a long pulse was only 2 mJ (pump energy contained in a diffraction limited core). This behavior was caused by a significant increase in the divergence of the S_1 radiation.

The results of its measurement at a short pump pulse are shown in Fig. 8*a*.

As seen from this figure, besides the increase in the S_1 divergence, the increase in the divergence of the passed pump radiation S_0 was also observed. This increase was caused, on the one hand, by the effect of “eating out” of the high-quality radiation and, on the other hand, by the appearance of a background due to light scattering. As the intensity of pump radiation decreased below the S_1 threshold, the divergence of the UV radiation passed through the cell (curve s_0) approached the divergence of the pump radiation. The divergence of S_1 and S_0 also decreased as the pump pulse duration increased from 20 to 120 ns (Fig. 8*b*). As the pump intensity increased, the divergence of S_1 in the latter case increased too (lower curve in Fig. 8*b*). To identify the factor that governs the divergence of S_0 and S_1 components, we have conducted a series of experiments with additional spatial filtration of radiation entering the cell (Fig. 9).

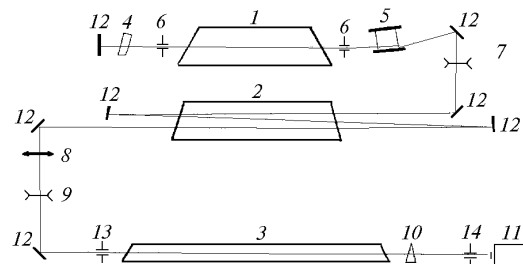


Fig. 9. Optical arrangement of the experiment with additional spatial filtration of the pump radiation: master oscillator 1; amplifier 2; cell filled with hydrogen 3; solid-state Fabry-Perot etalon 4; diffraction gratings 5; diaphragms 6, 13, 14; lenses 7, 8, 9 with $f = -80, 55, -20$ cm, respectively; a quartz wedge 10; an IMO-2N 11; total-reflection mirrors 12.

Figure 10 shows the photographs of the focal spots in S_0 and S_1 radiation components at different degrees of the pump beam vignetting. It follows from this figure that the divergence of S_1 depends, first of all, on the pump intensity, rather than on the degree of pump beam vignetting. Thus, near the threshold for S_1 occurrence, its divergence is close to the diffraction limited one. As the pump power increases, at the same input diaphragm aperture, the spot S_1 grows and becomes inhomogeneous. The decrease in the hydrogen pressure in this focusing geometry from 8 to 3 atm is almost equivalent to the decrease in the intensity of pump radiation.

Figure 11 shows time behavior of the intensity of vibrational Stokes components at short and long pump pulses. The presence of strong fluctuations of the intensity of the Stokes components and the passed pump radiation is typical, in spite of a relatively smooth profile of the incident radiation pulse. Besides, at short pump pulses we observed a marked shift of the intensity maxima of Stokes components with respect to the pump pulse.

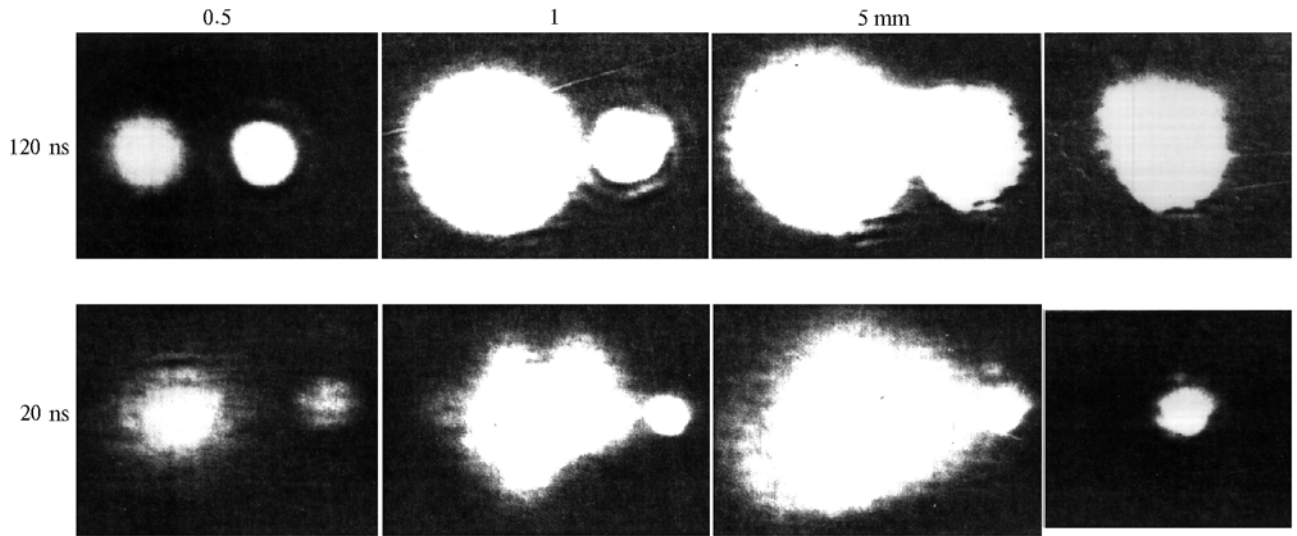


Fig. 10. Photographs of the spots of pump radiation (right-hand side) and S_1 at different diameters of the diaphragm 13 (shown by figures on the figure top) and pulse duration. The right-hand side pictures show the spots of the pump radiation without the beam vignetting diaphragm and without the cell with hydrogen.

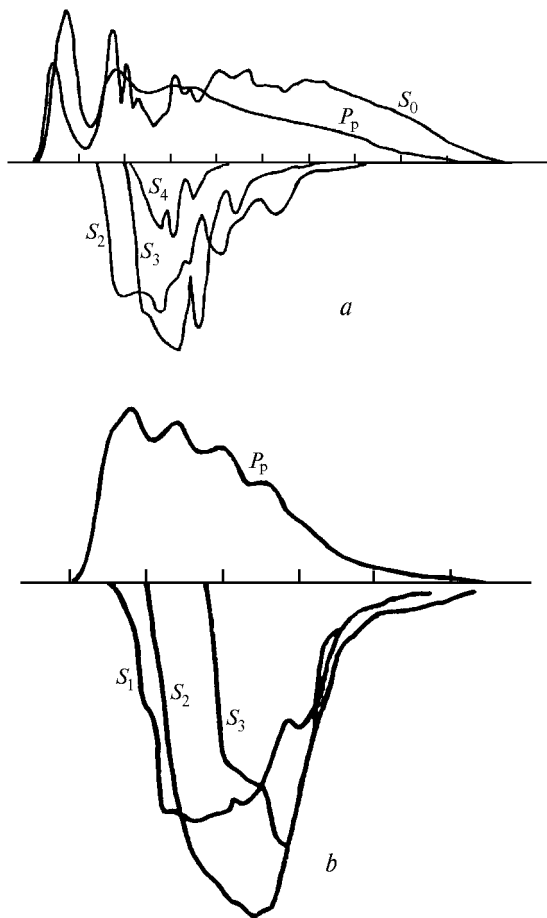


Fig. 11. Oscillograms of the pump radiation pulses (left) and Stokes vibrational components in the regime II (a) and III (b). The scale reads to 20 (a) and 10 ns (b).

4. Discussion

As known, the efficiency of the Raman parametric conversion of radiation strongly depends on the gain increment $G = I_p g l$ (l is the length of interaction). As a single-mode radiation is focused into a nonlinear medium, the increment G is independent of the focal length and equals to $2\pi g P_p / \lambda_p$ (P_p is the pump power). As seen from this equation, the increment can grow only if the pump power increases. At the same time, for efficient conversion the number of working particles in the interaction volume should be at least no less than the number of photons in the pump beam. This means that at low pressure of hydrogen (2–5 atm), which is needed to achieve the maximum value of g and the minimum line width of the scattered radiation, the efficient conversion is only possible at a long focusing length.

The below inequality for a single-mode beam follows from the condition of saturation in the number of particles within the interaction volume taking into account the size of the beam caustic:

$$(f/D)^4 \geq AP_p \tau / p \lambda_p^2, \tag{1}$$

where A is a constant; D is the initial diameter of the pump beam; p is the pressure of the working medium. As seen, the fulfillment of this inequality essentially depends on the ratio f/D or the numerical aperture of the focusing system, which is inversely proportional to this ratio. Under the conditions of our experiment, at the pressure of 3 atm the condition (1) means that the focal length f should be no less than 3 m.

Based on the above-said, the large number of rotational-vibrational components recorded in the

experiments is caused, in our opinion, by the following three factors: low divergence of the pump beam, low hydrogen pressure, and small numerical aperture of the focusing system. The high spatial coherence of the pump radiation and low hydrogen pressure allow the parameter γ to be close to the value optimal for amplification of the axial Stokes components on the vibrational transitions. For rotational components, the parameter γ is close to zero due to lower dispersion, and therefore the probability of appearance of the VSRS Stokes and anti-Stokes lines due to wave mixing is very high.¹ Besides, the strong interaction between the vibrational SRS components relates also the rotational components by the scheme shown in Fig. 12. Thus, even at a relatively low intensity of a vibrational Stokes component ($J = 1 \rightarrow J = 1$), the growth of the radiation intensity due to the transition $J = 1 \leftrightarrow J = 3$ is possible in its vicinity.

The experiments with the pump beam close to the collimated one have revealed a decrease in the efficiency of conversion into the higher vibrational Stokes components. As can be seen from Fig. 2b, in this case the conditions of occurrence of the higher Stokes components due to wave mixing retain in the regime I of operation of the laser system because of the high divergence of the pump radiation beam. At the minimum divergence of the pump beam (regimes II and III) purely Raman conversion is observed. However, in this case the divergence of the converted radiation essentially depends on whether or not the intensity of pump radiation exceeds the SRS threshold. Thus, at a long pump pulse (with the excess about 1.5 to 2), the divergence of S_1 is close to the geometric one determined by the caustic size. At higher intensity (short pulse) the divergence exceeds the geometric one by two to three times. Such a behavior is caused, first of all, by the stochastic nature of the stimulated scattering.^{15,16} This is also supported by the time behavior of the SRS components (see Fig. 11), which is characterized by strong intensity fluctuations.

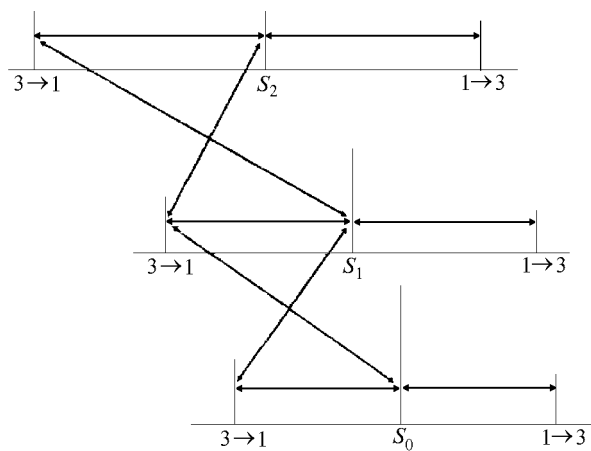


Fig. 12. Scheme of amplification of the VSRS lines in the process of wave mixing.

5. Conclusion

Thus, a great number of rotational-vibrational lines (about 70) were obtained in the process of conversion due to Raman scattering and wave mixing at single-frequency pumping of hydrogen by highly coherent XeCl-laser radiation. The stimulated radiation on the vibrational transitions has high degree of spatial and temporal coherence ($\Delta\nu = 0.01 \text{ cm}^{-1}$). Both these results were achieved owing to the use of low hydrogen pressure under the conditions favorable for Dicke effect of collisional narrowing to occur.

The high efficiency of conversion into the higher Stokes components and divergence of these components close to that of the pump radiation can be obtained only in the process of wave mixing under the mode locking conditions. In the case of only SRS without wave mixing, its cascade mechanism breaks down because of increasing divergence of the converted radiation in the field of the intense pump radiation.

Acknowledgments

The authors are thankful to Yu.N. Panchenko for the help in designing the pump laser systems.

References

1. L.L. Losev and A.P. Lutsenko, *Kvant. Elektron.* **20**, No. 11, 1054–1062 (1993).
2. I. Totaro, Y. Seiichi, K. Shuichi, and I. Nobuhiko, *Appl. Opt.* **32**, No. 33, 6633–6636 (1993).
3. N.V. Kravtsov and N.I. Naumkin, *Vestn. Mosk. Universiteta. Fizika. Astronomiya* **36**, No. 5, 84–87 (1995).
4. V.B. Morozov, A.N. Olenin, and V.G. Tunkin, *Kvant. Elektron.* **25**, No. 4, 293–294 (1998).
5. K. Hiroyuki, H. Yasuyuki, and I. Totaro, *IEEE J. Quantum Electron.* **34**, No. 2, 260–268 (1998).
6. G.V. Venkin, G.M. Krochik, L.L. Kulyuk, D.I. Maleev, and Yu.G. Khronopulo, *Zh. Eksp. Teor. Fiz.* **70**, No. 5, 1674–1685 (1976).
7. J.H. Newton and G.M. Shindler, *Opt. Lett.* **66**, No. 6, 125–129 (1981).
8. V.Yu. Baranov, V.M. Borisov, and A.Yu. Vinokhodov, *Kvant. Elektron.* **12**, No. 8, 1641–1649 (1985).
9. S.V. Mel'chenko, A.N. Panchenko, and V.F. Tarasenko, *Kvant. Elektron.* **13**, No. 7, 1496–1500 (1986).
10. M.R. Perrone, V. Piccino, G.De. Nunzino, and V. Nassasi, *IEEE J. Quantum Electron.* **33**, No. 6, 938–944 (1997).
11. A.F. Bokhanov, V.S. Burakov, A.S. Grabchikov, M.I. Nedel'ko, and V.A. Orlovich, *Zh. Prikl. Spektrosk.* **65**, No. 1, 67–74 (1998).
12. Yu.I. Bychkov, N.G. Ivanov, S.E. Kovalenko, V.F. Losev, Yu.N. Panchenko, and V.E. Prokop'ev, *J. of Russian Laser Research* **15**, 18–21 (1994).
13. N.G. Ivanov, S.E. Kovalenko, V.F. Losev, Yu.N. Panchenko, and V.E. Prokop'ev, *J. of Russian Laser Research* **17**, 401–405 (1996).
14. V.S. Starunov and I.L. Fabelinskii, *Usp. Fiz. Nauk* **98**, No. 3, 441–477 (1969).
15. V.I. Bespalov and G.A. Pasmannik, *Nonlinear Optics and Adaptive Laser Systems* (Nauka, Moscow, 1986), 134 pp.
16. B.Ya. Zel'dovich, N.F. Pilipetskii, and V.V. Shkunov, *Wave Front Inversion* (Nauka, Moscow, 1985), 247 pp.